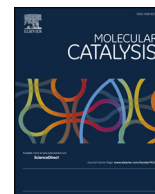




Contents lists available at ScienceDirect

Molecular Catalysis

journal homepage: www.elsevier.com/locate/mcat

Pd-Co catalysts prepared from palladium-doped cobalt titanate precursors for chemoselective hydrogenation of halonitroarenes

Tatiana M. Bustamante^a, Robinson Dinamarca^a, Cecilia C. Torres^b, Gina Pecchi^{a,c}, Cristian H. Campos^{a,*}

^a Departamento de Físico-Química, Facultad de Ciencias Químicas, Universidad de Concepción, Edmundo Larenas 129, Concepción, Chile

^b Departamento de Ciencias Químicas, Facultad de Ciencias Exactas, Universidad Andrés Bello, Sede Concepción, Autopista Concepción-Talcahuano 7100, Talcahuano, Chile

^c Millennium Nuclei on Catalytic Processes towards Sustainable Chemistry (CSC), Chile

ARTICLE INFO

Keywords:

Bimetallic catalyst
Supported catalyst
Cobalt
Palladium
Halonitroarenes

ABSTRACT

Bimetallic Pd-Co catalysts supported on the mixed oxides CoTiO₃-CoO-TiO₂ (CTO) were synthesized via the thermal reduction of Pd-doped cobalt titanates Pd_xCo_{1-x}TiO₃ and evaluated for the chemoselective hydrogenation of halonitroarenes to haloarene-amines. The nominal Pd mass percentage of the Pd-Co/CTO systems was varied from 0.0 to 0.50. After the thermal reduction of Pd_xCo_{1-x}TiO₃ at 500 °C for 3 h, Pd was completely reduced and Co was partially reduced, producing a mixture of ionic Co, metallic Co, and TiO₂-rutile species to give the supported bimetallic catalysts. The metallic cobalt content increased with the Pd content of the precursor. The catalytic activity toward 4-chloronitrobenzene increased with the Pd content; however, > 0.1 mass% Pd decreased the chemoselectivity toward 4-chloroaniline due to the formation of the hydrodehalogenation product—aniline. The 0.1Pd-Co/CTO system was used as a model catalyst to produce haloarene-amine building blocks for linezolid, loxapine, lapatinib, and sorafenib with > 98% conversion, 96% chemoselectivity, and no hydrohalogenation products. Finally, recycling tests of the 0.1Pd-Co/CTO catalyst showed loss of activity and selectivity during the third cycle due to catalyst deactivation. Regeneration treatments, every two catalytic cycles, allowed six operation cycles without loss of chemoselectivity and only a slight decrease in catalytic activity during the last cycle.

1. Introduction

The synthesis of compounds of interest in fine chemistry from reactions involving heterogeneous catalysts has been actively explored in recent years [1–4]. In particular, the production of haloaryl amines via processes involving the catalytic hydrogenation of halonitroarenes has proven to be an excellent synthetic strategy, and has allowed a series of building-block compounds for the preparation of molecules of pharmaceutical interest to be obtained [4–7]. To this end, a wide range of heterogeneous catalysts have been studied, with systems based on noble metals (NMs), such as Pt [8–12], Pd [13–17], Rh [18–20], Ir [21–23] and Au [24–27]. Among the systems based on NM active phases, supported Au catalysts have shown the best catalytic results, producing haloaryl amines in yields and selectivities of greater than 98%. Unfortunately, the use of NMs, and Au in particular, limits the large-scale potential of the resulting catalyst due to the high cost and limited natural abundance of NMs [4].

The non-NMs as Co have emerged as alternative active phases for the catalytic hydrogenation of halonitroarenes, and have shown promising selectivity for the production of haloaryl-amines [28–35]. However, these systems have the serious disadvantage of exhibiting low catalytic activity under mild reaction conditions (temperatures below 100 °C and hydrogen pressures below 20 bar), which necessitates the use of harsher operating conditions than those used for NM-based systems. A critical factor to improve the catalytic performance in the liquid-phase hydrogenation of halonitroarenes using metallic Co as active phase is the ability to control the surface chemistry of these materials to increase the activity, selectivity and operational stability. To remedy this drawback, the use of NM-Co bimetallic metal catalysts containing a very small amount of the NM (< 1% by mass with respect to the non-NM) has been reported [7,12,36]. Among NM, Pd is primarily used in most of the chemical industries because its low cost in compares with other NM as Rh, Pt and Au. The addition of Pd as a second metal on the non-NM based catalysts can significantly tailor the

* Corresponding author.

E-mail address: ccampos@udec.cl (C.H. Campos).

<https://doi.org/10.1016/j.mcat.2019.110702>

Received 17 September 2019; Received in revised form 25 October 2019; Accepted 28 October 2019

2468-8231/ © 2019 Elsevier B.V. All rights reserved.

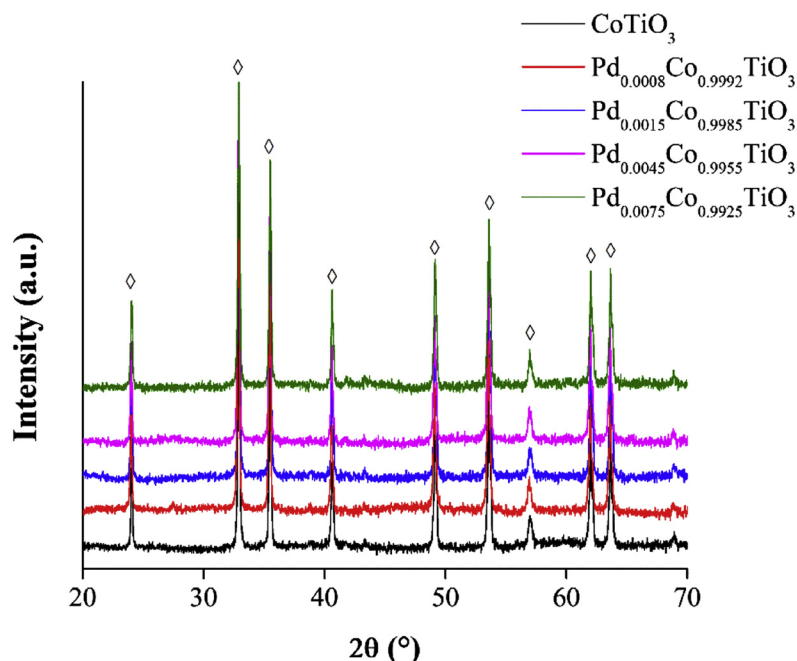


Fig. 1. X-ray diffraction patterns of the prepared $\text{Pd}_x\text{Co}_{1-x}\text{TiO}_3$ materials. \diamond - cobalt titanate (CoTiO_3) (ICDD 15-0866).

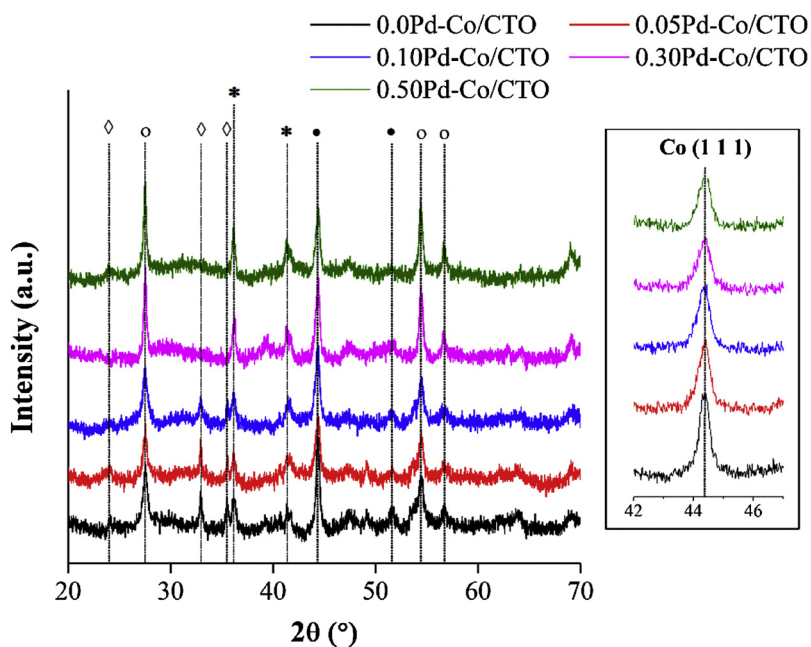


Fig. 2. X-ray diffraction patterns of the prepared $(\gamma)\text{Pd-Co/CTO}$ catalysts. Symbol key: \diamond - cobalt titanate (CoTiO_3) (ICDD 15-0866); \bullet - metallic Co (ICDD 15-0806); $*$ - hexagonal CoO (ICDD 78-0431); \circ - rutile TiO_2 (ICDD 03-065-1118). The inset shows an expansion of the area around $2\theta = 44^\circ$, which corresponds to the diffraction peak of metallic Co(1 1 1).

Table 1

Physiochemical characterization of the $(\gamma)\text{Pd-Co/CTO}$ catalysts prepared via the reduction of the $\text{Pd}_x\text{Co}_{1-x}\text{TiO}_3$ precursors.

Catalyst	AAS (%) ^a		d_{hkl} (nm)			H_2 -TPR reducibility ^b	S_{BET} ($\text{m}^2 \text{g}^{-1}$)
	% Pd	% Co	Co	CoO	CoTiO_3		
0.0Pd-Co/CTO	0.00	38.4 (38.0)	19.6	20	11.1	46	8
0.05Pd-Co/CTO	0.07 (0.04)	38.2 (37.8)	21.4	14.5	9.5	54	6
0.10Pd-Co/CTO	0.14 (0.12)	37.9 (37.8)	21.6	11.4	7.1	67	7
0.30Pd-Co/CTO	0.35 (0.29)	37.9 (37.6)	23.4	11.4	—	70	6
0.50Pd-Co/CTO	0.54 (0.48)	37.7 (37.4)	25.5	8.0	—	75	7

^a The contents of the metals in the $\text{Pd}_x\text{Co}_{1-x}\text{TiO}_3$ precursor are given in parenthesis.

^b Calculated from Eq. 1, which is provided in the Supplementary material.

electronic and geometric structures to enhance the catalytic performance including activity, selectivity, and the operational stability of catalyst system for the hydrogenation of the -NO₂ group [37–40].

This study reports the use of bimetallic Co-Pd catalysts containing a small amount of Pd as a dopant to promote their catalytic activity and chemoselectivity. The preparation of catalysts via the controlled reduction of a cobalt titanate precursor (Pd_xCo_{1-x}TiO₃) that includes a small amount of Pd as a promoter metal is reported for the first time. The resulting Pd-Co bimetallic catalysts are supported on the mixed oxides CoTiO₃-CoO-TiO₂ (CTO). The catalysts were designed to obtain systems of the type (y)Pd-Co/CTO (y = 0, 0.05, 0.1, 0.3, and 0.5% in Pd) to study the effects of the Pd content on their physicochemical properties and catalytic activity in the hydrogenation of liquid-phase halonitroarenes; 4-chloronitrobenzene (CNB) was used as a substrate for the production of 4-chloroaniline (CAN). The best catalytic system was evaluated in the hydrogenation of several halonitroarenes of pharmaceutical interest, namely, the 4-(2-fluoro-4-nitrophenyl) morpholine precursor of the antibacterial drug linezolid [41], the 1-(4-chlorophenoxy)-2-nitrobenzene precursor of the antipsychotic drug loxapine [42], the 2-chloro-1-((3-fluorobenzyl)oxy)-4-nitrobenzene precursor of the antineoplastic drug lapatinib, which is used in the treatment of breast cancer [43], methyl 2-chloro-5-nitrobenzoate, an intermediate in the synthesis of 3,4-dihydroquinolin-2(1H)-ones used in the treatment of type 2 diabetes [44], and the 1-chloro-4-nitro-2-(trifluoromethyl) benzene precursor of the antineoplastic drug sorafenib, which is used in the treatment of kidney cancer [45]. Finally, the best catalytic system was subjected to operational stability tests to evaluate its durability in continuous operation cycles.

2. Experimental

2.1. Materials

Cobalt(II) acetate (Co(CH₃CO₂)₂), titanium butoxide (Ti(CH₃CH₂CH₂CH₂O)₄), 4-chloronitrobenzene, 4-chloroaniline, 2-chloro-5-nitrobenzotrifluoride, methyl 2-chloro-5-nitrobenzoate, and 4-chloro-3-(trifluoromethyl)aniline were obtained from Sigma-Aldrich. Palladium(II) acetate (Pd(CH₃CO₂)₂), isopropanol, absolute ethanol, and ethylene glycol were purchased from Merck. All the purchased reagents were used without further purification. The gases H₂ (99.99%), He (99.99%), synthetic air, and nitrogen were provided by Linde Chile. The drug precursors 4-(2-fluoro-4-nitrophenyl) morpholine, 1-(4-chlorophenoxy)-2-nitrobenzene and 2-chloro-1-((3-fluorobenzyl)oxy)-4-nitrobenzene could not be sourced from commercial suppliers, so they were synthesized and characterized as detailed in the Supplementary material.

2.2. Synthesis of the Pd_xCo_{1-x}TiO₃ precursors

The synthesis of the precursors with the formula Pd_xCo_{1-x}TiO₃ was carried out using the methodology reported by Qu et al. with some modifications [46]. In general, the amounts of Co(CH₃COO)₂, Pd(CH₃COO)₂, and Ti(CH₃CH₂CH₂CH₂O)₄ required to achieve a molar ratio of (Co + Pd)/Ti = 1 were dissolved in an ethylene glycol/isopropanol (50/50) mixture. The nominal contents of Pd used corresponded to x = 0, 0.0008, 0.0015, 0.0045, and 0.0075. The above mixture was stirred for 24 h until a pinkish milky dispersion was obtained. Finally, the dispersion was stirred for 10 min and washed with absolute ethanol (×3) to remove excess ethylene glycol. The recovered solid was dried in an oven at 100 °C for 12 h and calcined in a static air atmosphere from room temperature to 700 °C at a heating ramp rate of 5° min⁻¹.

2.3. Synthesis of the (y)Pd-Co/CTO catalysts

The (y)Pd-Co/CTO catalysts with nominal Pd mass percentages (y)

of 0, 0.05, 0.1, 0.3, and 0.5% were synthesized using the methodology reported by Morales et al. [47]. The calcined material was subjected to an *ex situ* reduction treatment at 500 °C using H₂ as the reducing agent for 3 h. Subsequently, the catalyst was transferred to the reactor and quickly immersed in ethanol that had been previously degassed with N₂ to prevent its oxidation. The reduction temperature was chosen based on the H₂-TPR results.

2.4. Characterization

Chemical analysis was conducted via atomic absorption spectrometry (AAS) using a Perkin Elmer 3100 instrument. The samples were first evaluated in triplicate by digesting 0.05 g of the calcined Pd_xCo_{1-x}TiO₃ precursor or reduced (y)Pd-Co/CTO catalyst in 10 mL of a concentrated nitric/hydrochloric (1:3) acid solution via microwave-assisted digestion. After the reduction process, the Co and Pd metal loadings were measured using AAS.

Temperature programmed reduction (TPR) was performed using a TPR/TPD 2900 Micromeritics system with a thermal conductivity detector (TCD). Two reduction measurement profiles were recorded. In the first (H₂-TPR1), TPR data was recorded for 0.050 g samples of the calcined Pd_xCo_{1-x}TiO₃ precursors using a 5% H₂/Ar flow of 40 mL min⁻¹ and a heating rate of 10 °C min⁻¹ from room temperature to 800 °C. In the second (H₂-TPR2), 0.050 g samples of the calcined Pd_xCo_{1-x}TiO₃ precursors were first thermally reduced in the TPR-equipment using the same experimental conditions as in the preparation of the (y)Pd-Co/CTO materials (pure H₂ flux of 30 ml/min, heating from room temperature to 500 °C at 10 °C/min). After the reducing treatment, the samples were cleaned at 100 °C under an Ar flow for 2 h, and TPR data from a second run using the H₂-TPR1 conditions was recorded. Thus, the H₂-TPR1 data represented the complete reduction of the Co species in the precursor materials, and the H₂-TPR2 data represented Co reduction in the prepared (y)-Pd-Co/CTO catalysts. The reducibility was calculated from the H₂-TPR data as follows:

$$\text{reducibility (\%)} = \frac{\text{Total normalized area of } H_2 - \text{TPR2}}{\text{Total normalized area of } H_2 - \text{TPR1}} \cdot 100 \quad (1)$$

In this expression, the peak areas were normalized by the total experimental Co content determined using AAS characterization.

The specific areas were calculated using the BET method from N₂ adsorption-desorption isotherms obtained at -196 °C using a Micromeritics TriStar II 3020. X-ray powder diffraction (XRD) patterns of the as-synthesized powder samples were obtained with nickel-filtered CuK_{α1} radiation (λ = 1.5418 Å) using a Rigaku diffractometer, and were collected over the 2θ range 20-90°. The reduced (y)Pd-Co/CTO catalyst samples were subjected to a passivation treatment prior to XRD to avoid continued oxidation during the XRD measurement. The details of the passivation treatment have been described in our previous reports [47].

Transmission electron microscopy (TEM) micrographs were obtained using a JEOL model JEM-1200 EX II microscope; the materials were dispersed on a carbon grid. The reduced (y)Pd-Co/CTO catalysts were subjected to the passivation treatment prior to TEM characterization.

X-ray photoelectron spectroscopy (XPS) was performed using a VG Escalab 200R electron spectrometer equipped with a hemispherical electron analyzer and a Mg K_α (1253.6 eV) X-ray source. The calcined Pd_xCo_{1-x}TiO₃ precursor samples were measured without prior reducing treatment. The reduced (y)Pd-Co/CTO catalysts were reduced *in situ* in the XPS pre-chamber prior to analysis. Finally, magnetic characterization of the nanomaterials was carried out using a Quantum Design Dynacool Physical Properties Measurement System (PPMS) equipped with a vibrating sample magnetometer (VSM). Magnetization curves were only obtained for the (y)Pd-Co/CTO reduced catalysts, which were passivated prior to analysis, at 27 °C. Data is reported in emu per gram of Co. M_S was evaluated by extrapolating the experimental results

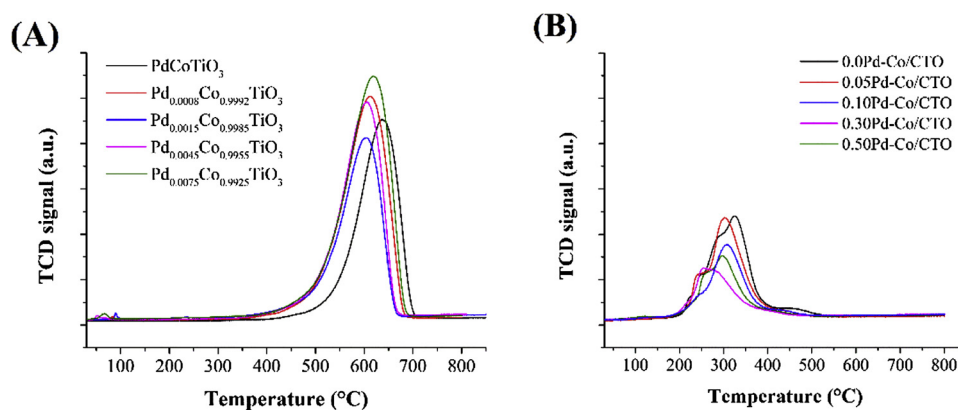


Fig. 3. H₂-TPR profiles for the synthesized materials. (A) H₂-TPR1 results for the Pd_xCo_{1-x}TiO₃ precursors and (B) H₂-TPR2 results corresponding to the reduction of (y)Pd-Co/CTO reduced catalysts.

Table 2
Magnetic and XPS characterization of the (y)Pd-Co/CTO catalysts.

Label	M_s (emu g ⁻¹)	H_c (Oe)	Binding energy (eV)			Surface atomic ratio	
			Co 2p _{3/2}	Pd 3d _{5/2}	Ti 2p _{3/2}	Co/Ti	Pd/Ti
CoTiO ₃	—	—	781.2	—	457.9	1.02	—
Pd _{0.0008} Co _{0.9992} TiO ₃	—	—	781.0	trace	458.1	1.00	—
Pd _{0.0015} Co _{0.9985} TiO ₃	—	—	781.0	338.0	458.0	0.97	0.0001
Pd _{0.0045} Co _{0.9955} TiO ₃	—	—	781.1	338.1	457.9	1.04	0.0025
Pd _{0.0075} Co _{0.9925} TiO ₃	—	—	781.2	337.9	458.1	0.99	0.0089
0.0Pd-Co/CTO	141.8	302.8	777.7 (21) 780.1 (79)	—	457.9 (84) 455.5 (16)	0.94	—
0.05Pd-Co/CTO	142.4	520.8	778.2 (32) 781.4 (68)	trace	458.5 (78) 455.9 (22)	0.90	—
0.10Pd-Co/CTO	148.6	477.2	777.9 (40) 780.6 (60)	335.2	458.4 (83) 455.9 (17)	0.92	0.0002
0.30Pd-Co/CTO	150.7	481.4	777.9 (53) 780.6 (47)	335.1	458.4 (90) 456.2 (10)	0.85	0.0031
0.50Pd-Co/CTO	148.1	443.0	778.0 (61) 782.7 (39)	335.2	459.3 (100)	0.83	0.0078

obtained in the high field range, in which the magnetization increases linearly with $1/H$, to infinite field.

2.5. Catalytic activity

The catalytic activity of the (y)Pd-Co/CTO systems in the hydrogenation of halonitroarenes was evaluated using 0.030 g of catalyst and the necessary amount of substrate to obtain a mol_{substrate} : mol_{metal(Pd+Co)} ratio of 100, based on the quantities of metals determined from AAS, TPR, and XPS characterization. All activity measurements were performed in triplicate using a Parr Model 5513 reactor with mechanical agitation to which 40 mL of ethanol was added at a H₂ pressure of 10 bar at 80 °C. The reaction products were identified via gas chromatography using a GC Hewlett Packard HP 4890 D instrument equipped with an HP-5 capillary column and a flame ionization detector (FID). The conversion and selectivity were calculated using calibration curves and the following equations:

$$X_{\text{substrate}} (\%) = \frac{[\text{substrate}]_i - [\text{substrate}]_f}{[\text{substrate}]_i} \cdot 100 \quad (2)$$

$$S_{\text{product}} (\%) = \frac{[\text{product}]_f}{[\text{substrate}]_i - [\text{substrate}]_f} \cdot 100 \quad (3)$$

For the hydrogenation reaction of the pharmaceutical intermediate substrates, the same operational conditions were used as in the CNB reaction. The products of all the reactions were followed using a gas chromatograph coupled to a mass detector (Perkin Elmer GCMS-SQ8T).

3. Results and discussion

3.1. Characterization of the materials and catalysts

XRD was used to confirm the formation of the cobalt titanate-based materials; the results are shown in Fig. 1. In the Pd_xCo_{1-x}TiO₃ systems, the diffraction profile of the CoTiO₃ ilmenite structure (ICDD 15-0866) was present. The incorporation of Pd did not result in the appearance of segregated phases of PdO_x, TiO_x, or Co_xO_y, which could be attributed to a high tolerance to the incorporation of Pd by the CoTiO₃ structure or the segregation of highly dispersed metal oxide phases that were not detected by XRD in the CoTiO₃ structure.

Fig. 2 shows the XRD patterns of the reduced (y)Pd-Co/CTO catalysts. All systems showed diffraction peaks characteristic of the crystalline phases of metallic Co (ICDD 15-0806), rutile TiO₂ (ICDD 03-065-1118), and CoO (ICDD 78-0431), in agreement with the report of Hwang et al. for CoTiO₃ oxidation-reduction cycles [48]. After the reduction treatment, diffraction peaks corresponding to CoTiO₃ were only observed in the (y)Pd-Co/CTO systems with $y = 0.0, 0.05,$ and 0.10 ; this was attributed to incomplete reduction of the Pd_xCo_{1-x}TiO₃ precursor ($x = 0.0008, 0.0015$ and 0.0045). However, the catalysts (y)Pd-Co/CTO systems with $y = 0.30$ and 0.50 showed only the presence of CoO and TiO₂-rutile on the catalysts structure. We suggest this effect to the increase of the Pd loading on the catalysts surface which could promote the Pd_xCo_{1-x}TiO₃ precursor reducibility (see below in TPR characterization). Signals corresponding to the presence of PdO_x or metallic Pd were not detected in any of the doped catalysts; we assumed that the Pd species had formed aggregates with crystal sizes below the

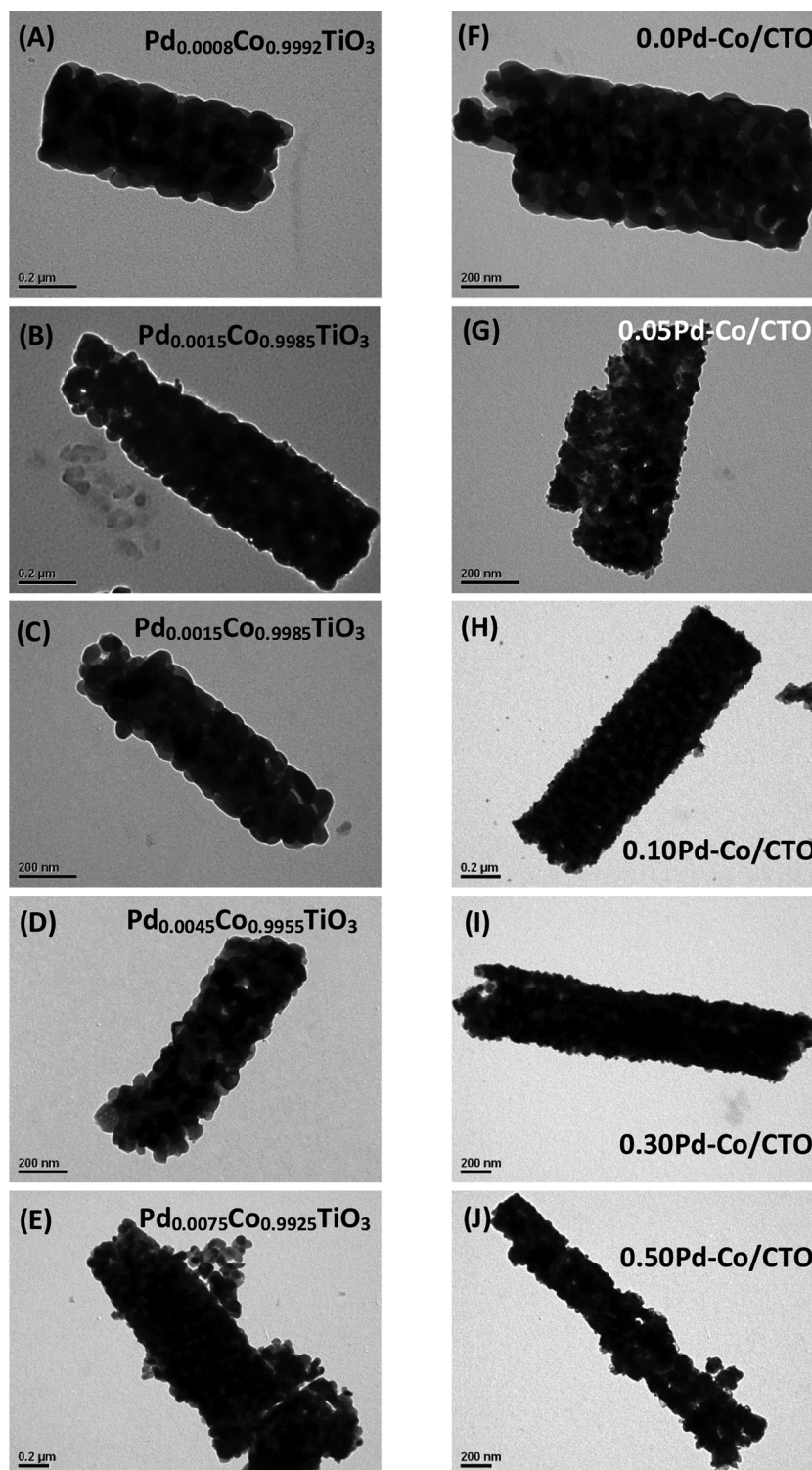


Fig. 4. TEM micrographs of (A–E) the $\text{Pd}_x\text{Co}_{1-x}\text{TiO}_3$ precursors and (F–J) the reduced $(\gamma)\text{Pd-Co/CTO}$ catalysts.

limit of detection. The chemical nature of the active phase was investigated using the metallic Co diffraction peak corresponding to the index $hkl(111)$; as shown in the inset of Fig. 2, this peak was not shifted toward the lower angle range with respect to that of pure Co in the catalysts, ruling out the formation of Pd-Co alloys during the reduction treatment [49]. Finally, the crystal sizes of the metallic Co, CoTiO_3 , and CoO were calculated using the diffraction peaks corresponding to (111) , (104) , and (111) , respectively, via the Scherrer equation; the obtained values are summarized in Table 1. The

incorporation of Pd into the $\text{Pd}_x\text{Co}_{1-x}\text{TiO}_3$ materials increased the crystal size of the metallic Co particles. This behavior consistent with the decreased crystal size of CoO and disappearance of the CoTiO_3 diffraction peaks, which were attributed an increased degree of Co reduction in the obtained catalysts.

To complement the XRD characterization, the temperature-programmed reduction (H_2 -TPR) curves were obtained for the $\text{Pd}_x\text{Co}_{1-x}\text{TiO}_3$ precursors (H_2 -TPR1, Fig. 3A) and the reduced $(\gamma)\text{Pd-Co/CTO}$ catalysts (H_2 -TPR2, Fig. 3B). In the CoTiO_3 system, only one reduction

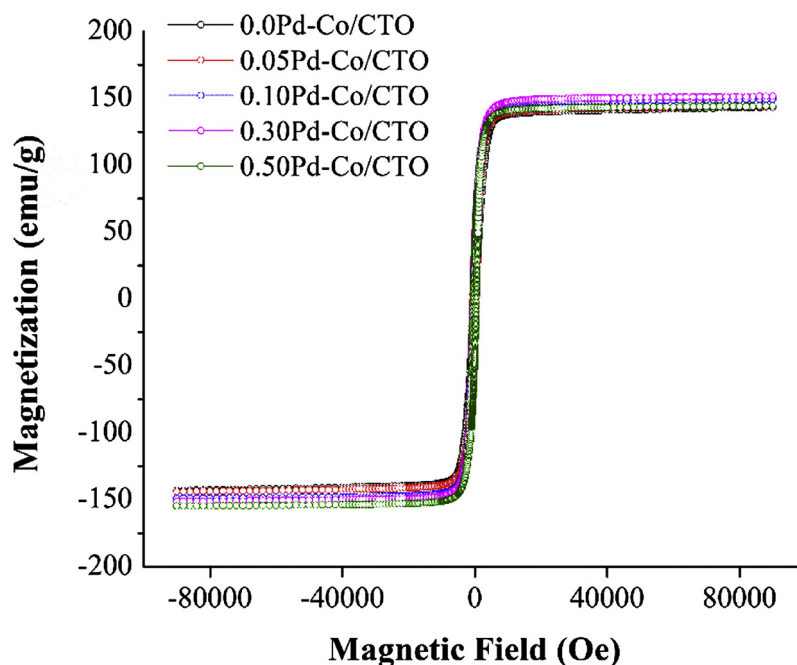


Fig. 5. Vibrating sample magnetometry (VSM) analysis of the (γ)Pd-Co/CTO catalysts.

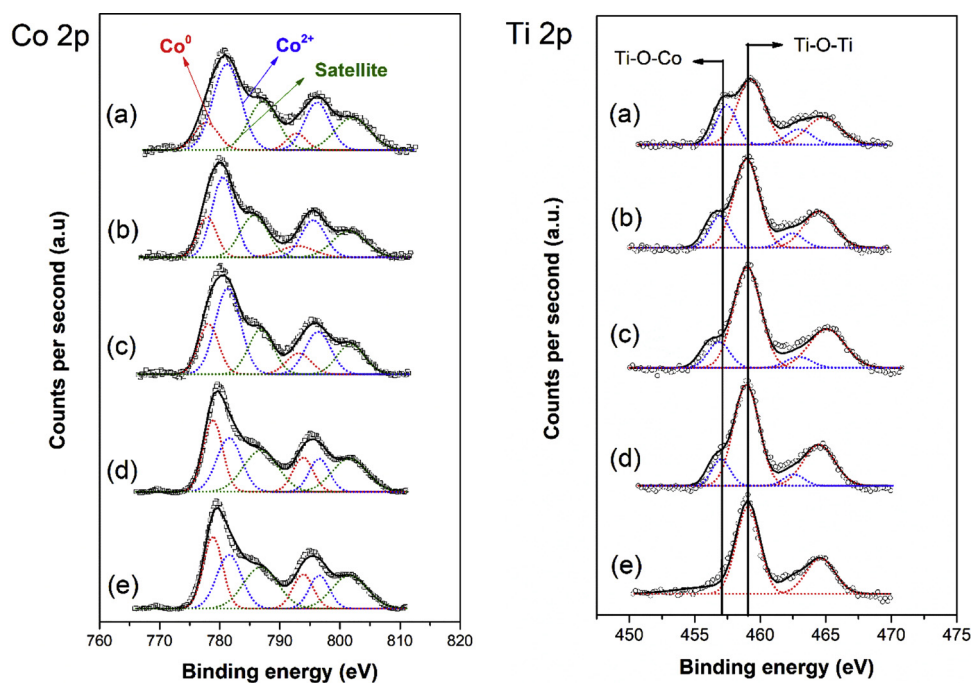


Fig. 6. XPS spectra of the (γ)Pd-Co/CTO reduced catalysts. (a) 0.0Pd-Co/CTO, (b) 0.05Pd-Co/CTO, (c) 0.10Pd-Co/CTO, (d) 0.30Pd-Co/CTO, and (e) 0.50Pd-Co/CTO.

signal was observed at approximately 550 °C, and was attributed to the reduction of the ionic Co embedded in the crystal lattice of the cobalt titanate to CoO_x species and subsequently to metallic Co in a single step. For the $\text{Pd}_x\text{Co}_{1-x}\text{TiO}_3$ systems with $x = 0.0008\text{--}0.0075$, two reduction stages were observed: the first at approximately 75–100 °C was attributed to the reduction of the ionic Pd species to metallic Pd, and the second at below 550 °C corresponded to the reduction of the cobalt in the CoTiO_3 structure. As the content of Pd in the CoTiO_3 structure was increased, two phenomena were observed: (i) A shift in the temperature of the higher-temperature Co ionic reduction peak and (ii) an increase in the area under the curve of the H_2 -TPR1 reduction signal. These behaviors could be attributed to the emergence of metallic Pd clusters,

which could promote the chemisorption of H_2 and thus favor the reduction of cobalt in the $\text{Pd}_x\text{Co}_{1-x}\text{TiO}_3$ structure by hydrogen spill-over effect.

To determine the metallic cobalt content in the catalysts, the H_2 -TPR2 analysis program was applied; the results are shown in Fig. 3B. The reduction profiles showed behavior similar to that observed in the H_2 -TPR1 results in terms of the displacement of the reduction signal to lower temperature with increasing Pd content. However, in contrast to the increased signal areas observed in H_2 -TPR1, the area under the H_2 -TPR2 signals decreased with increasing Pd content. This behavior could be explained as a combined effect of the nature of the oxides produced during the thermal treatment with H_2 (mainly CoO and TiO_2) and the

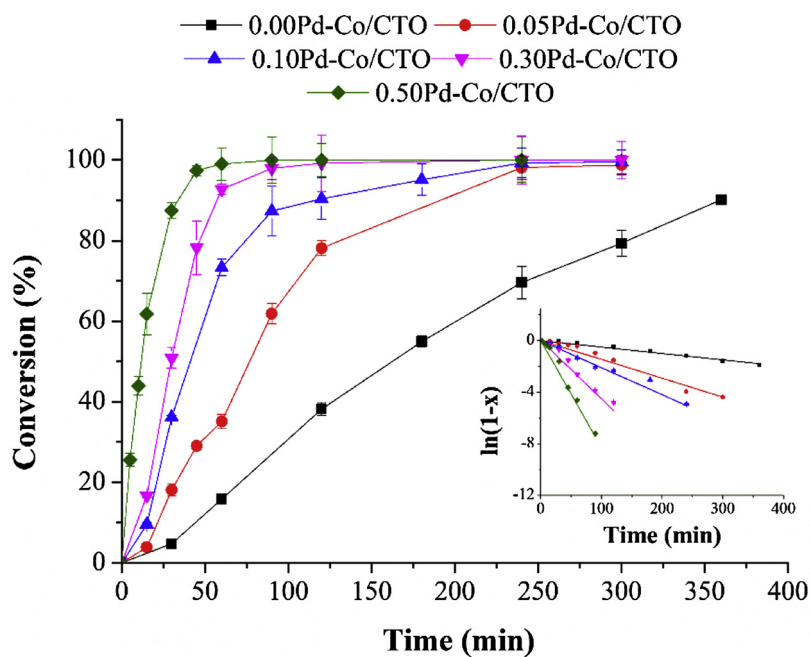
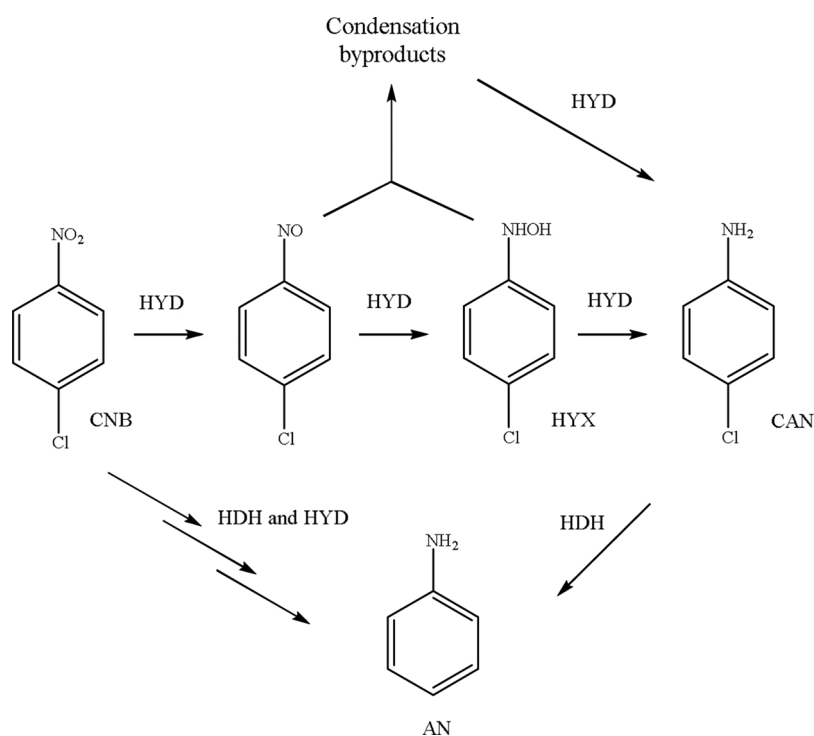


Fig. 7. Conversion as a function of time in the hydrogenation of CNB using the (y)Pd-Co/CTO catalysts. Inset: fitting using the kinetic pseudo-first-order model.



Scheme 1. Reaction pathways of the hydrogenation (HYD) and/or hydrodehalogenation (HDH) of CNB.

amount of metallic Pd and Co available in the catalysts after the reduction treatment. Notably, no reduction signals were observed around 100 °C, which suggested that the ionic Pd species were completely reduced during the reduction process at 500 °C.

The degree of reducibility of the cobalt was calculated from the H₂-TPR1 and H₂-TPR2 profiles, as summarized in Table 1. The trend shows that approximately 45% of the cobalt was reduced during the reduction treatment in the 0.0Pd-Co/CTO system; with increasing Pd content, the amount of metallic cobalt in the (y)Pd-Co/CTO catalysts with $y = 0.05$ – 0.5 increased. Importantly, this trend was also in agreement with the metallic crystal sizes determined using XRD (see Table 1). In

the H₂-TPR1 analysis, the first stage of reduction corresponded to the formation of Pd clusters, which were believed to be highly dispersed because they were not detected via XRD (size < 5.0 nm). These Pd nanocrystals were responsible for the increased reduction of the oxidized Co species, as well as the increase in the size of the cobalt metal clusters with increasing Pd content in the Pd_xCo_{1-x}TiO₃ structure (see Table 2). These results demonstrate that (i) reduction at 500 °C for 3 h produced greater than 45% metallic cobalt in all the systems studied; (ii) the incorporation of the Pd promoted the reduction of the cobalt in the cobalt titanate precursor, reaching a maximum of 75% in the 0.50Pd-Co/CTO system; and (iii) increased Pd content promoted the

Table 3

Time required to reach 100% conversion, initial reaction rate, global pseudo-first order constant, and selectivity toward CAN and AN of the Pd-Co/CTO catalysts.

Catalyst	t (min)	v_0^a (mmol L ⁻¹ min ⁻¹)	k_{global}^a (min ⁻¹ g _{metallic Co} ⁻¹)	Selectivity (%) ^b		
				CHX	CAN	AN
0.0Pd-Co/CTO	600	0.23	0.04	1.9	98.1	—
0.05Pd-Co/CTO	300	1.19	0.22	2.0	98.0	—
0.10Pd-Co/CTO	240	2.60	0.49	—	100	—
0.30Pd-Co/CTO	120	7.78	1.47	—	94.4	5.6
0.50Pd-Co/CTO	60	17.6	3.36	—	84.8	15.2

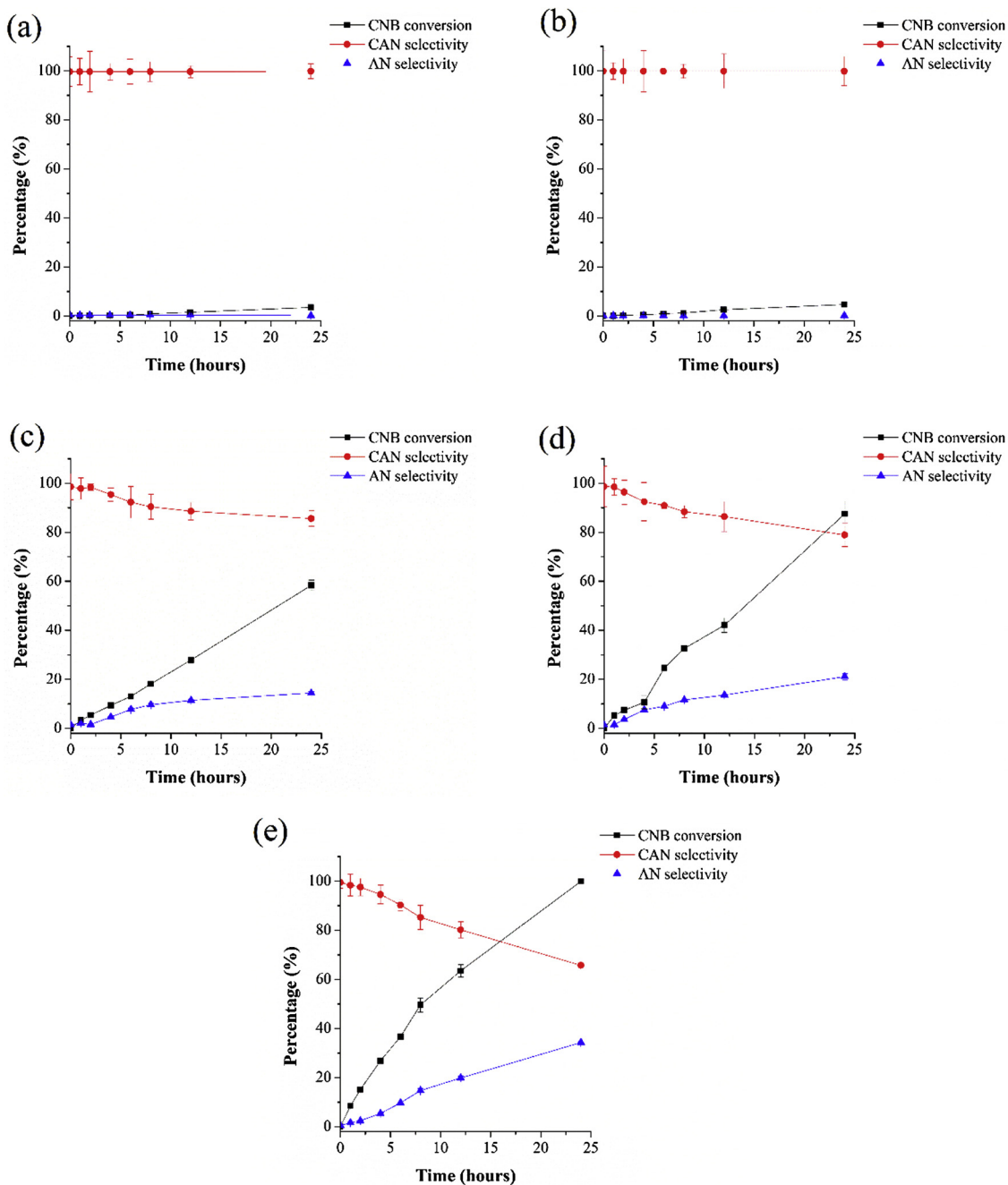
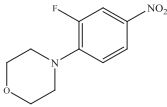
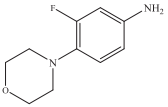
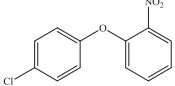
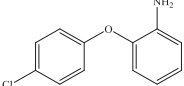
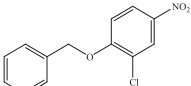
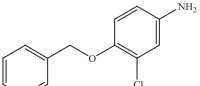
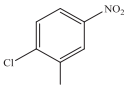
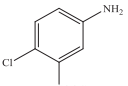
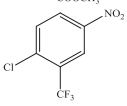
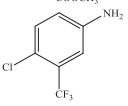
^a Calculated from the AAS, TPR and XPS characterization for metallic Co and v_0 at 10% of CNB conversion level.^b Calculated at 100% CNB conversion.**Fig. 8.** Conversion and selectivity for CNB hydrogenation using the Pd_xCo_{1-x}TiO₃ precursor materials as catalysts. All experiments were performed using the same reaction conditions employed in the experiments with the (γ)Pd-Co/CTO catalysts.

Table 4

Conversion and selectivity of the hydrogenation of halonitroarenes over the 0.10Pd-Co/CTO catalyst. (10 bar H₂, 80 °C, 0.030 g of catalyst, substrate/metallic Co mole ratio of 100, 50 mL of ethanol, 750 rpm).

Entry	Substrate	Time (min)	X (%)	Selectivity (%)
1		120	97	 > 99
2		360	96	 > 99
3		420	97	 95 ^a
4		120	99	 > 99
5		60	99	 > 99

^a Only 4-amino-2-chlorophenol and 1-fluoro-3-methylbenzene were detected as by products.

formation of smaller cobalt crystals during the reduction treatment.

N₂ adsorption-desorption isotherms were obtained at -196 °C for the Pd_xCo_{1-x}TiO₃ precursors and reduced (y) Pd-Co/CTO catalysts. All the isotherms were classified as type III according to the IUPAC classification scheme (see Figs. S1 and S2 in Supplementary material). The apparent specific surface values were calculated using the Brunauer-Emmett-Teller (BET) methodology, and the values obtained are summarized in Table 1. All the prepared systems (both precursors and reduced catalysts) showed S_{BET} values of 6–7 m²g⁻¹, which are characteristic of non-porous materials.

The TEM images of all the materials are shown in Fig. 4. The Pd_xCo_{1-x}TiO₃ precursors formed micro-rods via agglomeration of oriented micro- and nanoparticles of Pd_xCo_{1-x}TiO₃; the rods grew one-dimensionally to reach average sizes of 500–550 nm with widths of 90–120 nm (Fig. 4A–E).

The reduction treatment did not significantly change the shape or dimensions of the micro-rods, as shown in Fig. 4F–J. The only change after reduction was the increased contrast of the images, which was attributed to the appearance of metallic Co and Pd in the reduced (y)Pd-Co/CTO catalysts, as observed by XRD and H₂-TPR.

The reduced (y)Pd-Co/CTO catalysts had metallic Co contents between 40 and 75%, depending on the Pd content. For this reason, we decided to perform VSM characterization at room temperature to determine the magnetic properties of the obtained catalysts. Fig. 5 shows that all the catalysts exhibited magnetization curves of typical ferromagnetic materials. The estimated values of saturation magnetization (M_s) and coercivity (H_c) are summarized in Table 2. Based on the ferromagnetic behavior of the catalysts, we expected that they could be easily separated from the reaction medium using an external magnetic field [50]. An experimental test confirmed that it was indeed possible to separate the solid from the reaction medium with 1 min using a magnet.

XPS characterization was performed to determine the oxidation states of the constituents of the synthesized materials. A summary of the obtained data is shown in Table 2. The Co 2p_{3/2}, Ti 2p_{3/2}, and Pd 3d_{5/2} binding energies (BEs) of the Pd_xCo_{1-x}TiO₃ materials and (y)Pd-Co/CTO reduced catalysts were compared (Fig. S3 in the Supplementary material). All the Pd_xCo_{1-x}TiO₃ precursor spectra showed only Co²⁺ species at a BE of 781 eV, which was attributed to the Co species in the cobalt titanate network [48,51,52]. In the Ti 2p_{3/2} region, only a contribution

at ~458 eV was observed, which was attributed to Ti-O-Co species [51]. This result correlated with the formation of the CoTiO₃ structure in the materials, confirming the results obtained using XRD. Finally, we determined that the oxidation state detected for Pd 3d_{5/2} corresponded to Pd⁴⁺ (BE = ~338.0 eV), allowing us to infer that the reduction observed in the H₂-TPR1 analyses of the Pd_xCo_{1-x}TiO₃ materials corresponded to the transformation of Pd⁴⁺ into metallic Pd. The atomic ratios of the Co, Pd, and Ti species on the surfaces of the materials are summarized in Table 2. All systems had a Co/Ti surface ratio of approximately 1, which was in agreement with the stoichiometry of the prepared materials. However, the Pd/Ti atomic ratio increased with the Pd content in the catalyst structure, and the values were higher than the nominal values of the formulations from which they were prepared. This suggested that Pd was highly dispersed as PdO₂ on the surface of CoTiO₃ during the synthesis of the materials [53,54].

The Co 2p spectra of the (y)Pd-Co/CTO reduced catalysts are shown in Fig. 6. This signal has been used to estimate the contribution of metallic Co species at a BE of 778 eV and ionic Co at a BE of 781–782 eV (Fig. 6A) [51]. A summary of the contributions is given in Table 2; an increase in the metallic Co species was observed as the Pd content of the catalyst formulation was increased. In all the Pd-doped systems, only one Pd 3d_{5/2} peak with a BE of 335.2 eV was detected, which confirmed the complete reduction of Pd during the reduction treatment and ruled out the formation of Pd-Co alloys [55,56]. This information confirmed the results obtained from the H₂-TPR2 characterization, in which no reduction signals attributed to palladium ionic species were observed for the (y)Pd-Co/CTO reduced catalysts with y > 0.0.

In the Ti 2p_{3/2} region, the appearance of a second signal at a BE of 458.3 eV was observed and attributed to the formation of Ti–O–Ti species during the reduction treatment [51,57], as shown in Fig. 6. The contributions of the Ti–O–Ti species increased with the Pd content; as observed in the XRD characterization, the Pd promoted the reduction of the Co in CoTiO₃, leading to the formation of rutile TiO₂.

3.2. Catalytic activity

3.2.1. Effect of the Pd content on the activity of the reduced (y)Pd-Co/CTO catalysts

The catalytic activities of the reduced (y)Pd-Co/CTO systems are

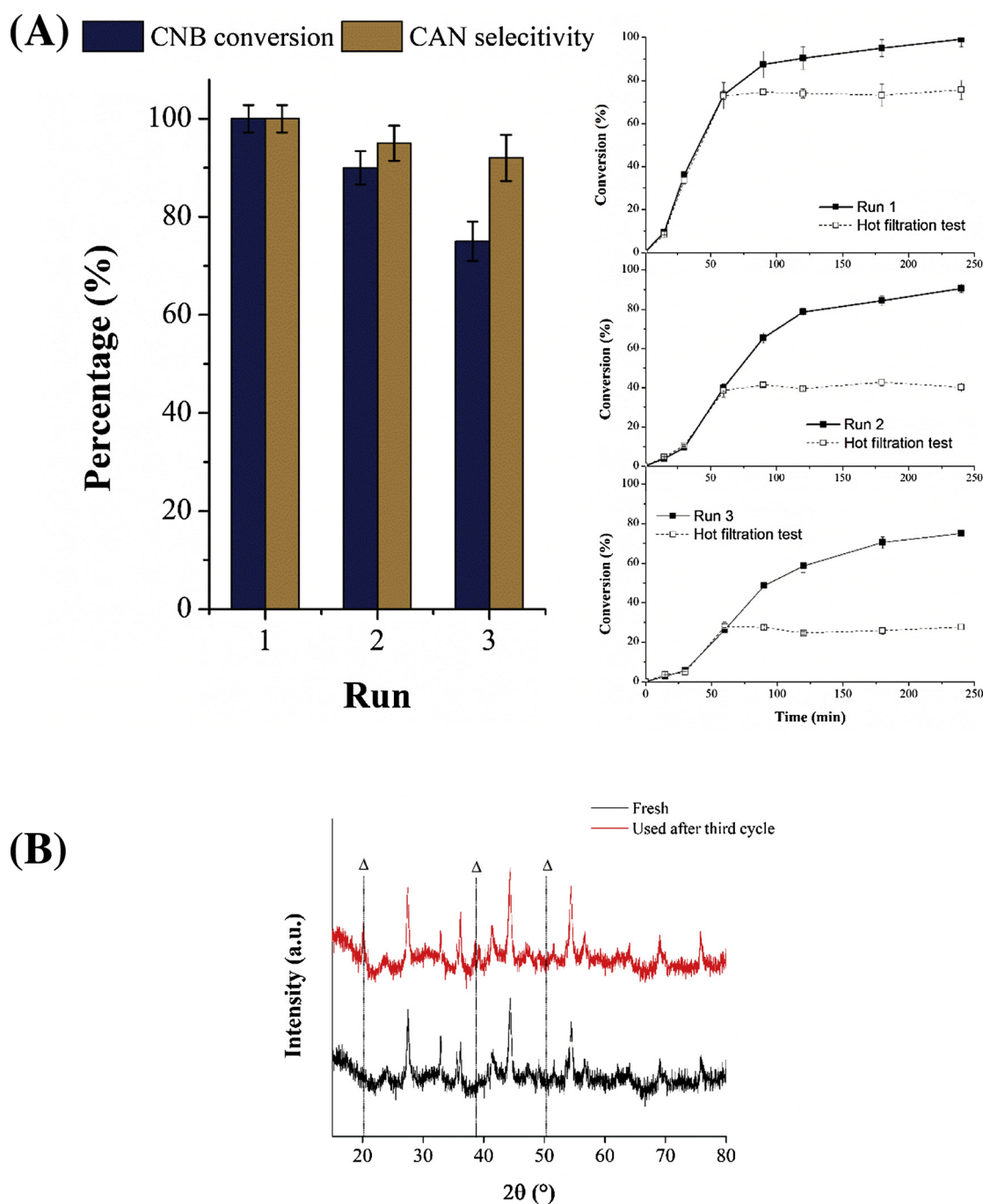


Fig. 9. Recycling test of the reduced catalyst (0.10Pd-Co/CTO) in CNB hydrogenation. (A) Conversion of CNB and the selectivity toward CAN as a function of the number of operation cycles. The inset of (A) corresponds to the catalyst filtrate tests obtained between operation cycles after 60 min of reaction. (B) XRD characterization of the catalyst recovered after the third operation cycle (Δ - CoOOH (ICDD 78-0431)).

shown in Fig. 7. The (γ)Pd-Co/CTO catalysts showed pseudo-first-order conversion kinetics with respect to CNB consumption over time. Because the studied catalysts had low surface areas ($\sim 40 \text{ m}^2 \text{ g}^{-1}$), we assumed that the Pd⁰ and Co⁰ species at the surface (as determined using TPR and XPS) represented all the metal available for the catalytic reaction. When Pd was incorporated into the catalyst structure, a significant increase in the initial reaction rate was observed. In terms of the selectivity of the reaction, the catalyst 0.10Pd-Co/CTO produced the desired product CAN; additionally, some accumulation of the reaction intermediate N-(4-chlorophenyl)-hydroxylamine (HYX) was observed (see Scheme 1).

As the Pd content of the reduced (γ)Pd-Co/CTO catalysts was

increased, two effects were observed: (i) The disappearance of the HYX intermediate and (ii) the appearance of the hydrodehalogenation (HDH) product AN, which was significant for the 0.30Pd-Co/CTO and 0.50Pd-Co/CTO catalysts (see Table 3). The presence of AN in the reaction mixture was attributed to the HDH of the product CAN, as observed in the distribution curves of the reaction products (Fig. S4 in the Supplementary material).

To evaluate the effect of Pd on the HDH activity in the reaction of CNB, the Pd_xCo_{1-x}TiO₃ catalyst precursors were evaluated under the same operating conditions; the results are shown in Fig. 8. Although the catalysts were not previously reduced, the H₂-TPR1 results indicated that the available Pd in the precursors could be reduced at a H₂ pressure

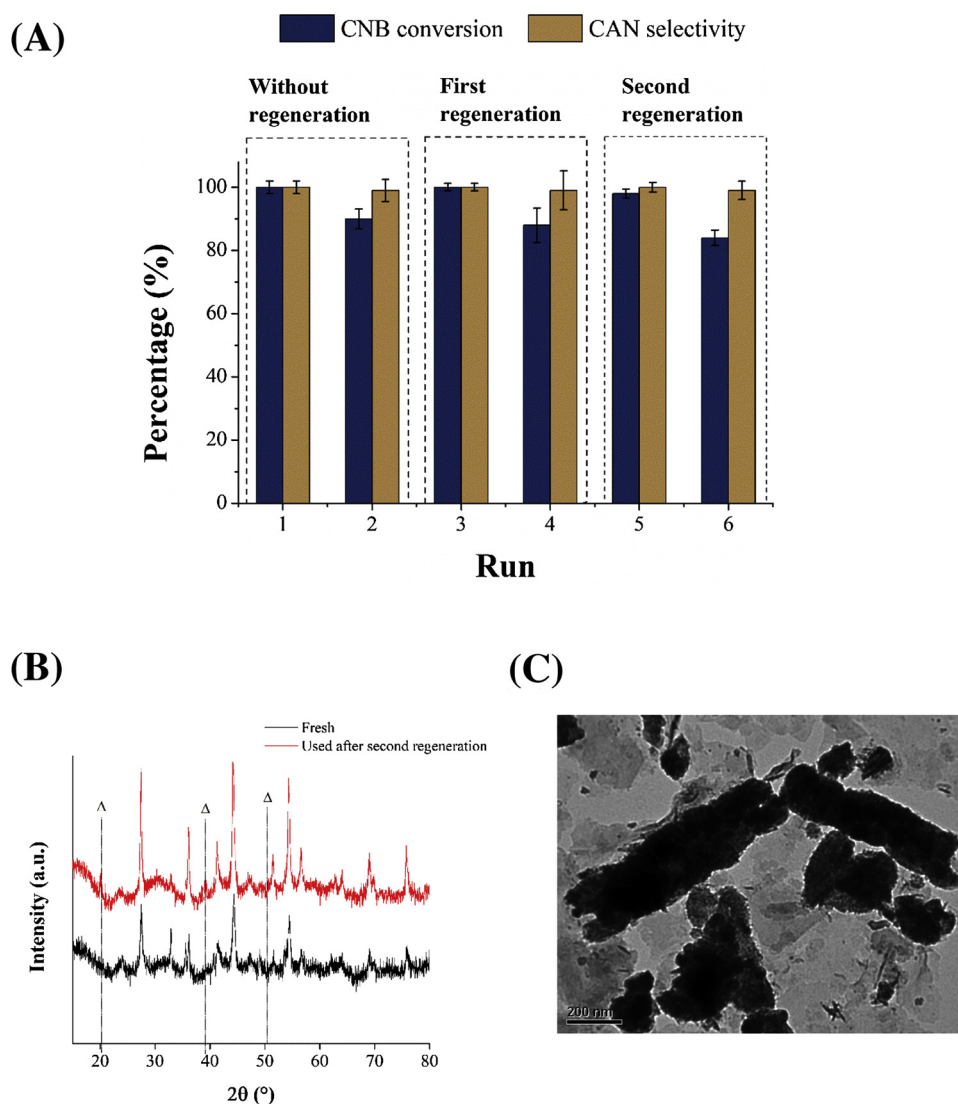


Fig. 10. Results of the regeneration of the reduced 0.10Pd-Co/CTO catalyst after every second operation cycles in CNB hydrogenation. (A) Conversion of CNB and selectivity toward CAN as a function of the operation cycle number. (B) XRD (left) and TEM (right) characterization of the recovered catalyst after the sixth operation cycle (Δ - CoOOH (ICDD 78-0431)).

of 10 bar at 80 °C, as has been reported in the literature by some authors [58–60].

In the $\text{Pd}_x\text{Co}_{1-x}\text{TiO}_3$ systems with $x = 0.0$ and 0.0008 (which are precursors of the $(\gamma)\text{Pd-Co/CTO}$ systems with $y = 0.0$ and 0.05, respectively), very low catalytic activities were observed (~5% conversion) with 99.9% selectivity toward the product of interest. However, the $\text{Pd}_x\text{Co}_{1-x}\text{TiO}_3$ systems with $x = 0.0015$, 0.0045, and 0.0075 (which were precursors of the $(\gamma)\text{Pd-Co/CTO}$ systems with $y = 0.10$, 0.30, and 0.50, respectively) showed greater activities, reaching conversions higher than 50% at 24 h of reaction with selectivities of 85%, 78%, and 65% toward CAN, respectively. In all the catalytic tests, CAN and AN were the only reaction products detected.

The results obtained from the activity tests of the $\text{Pd}_x\text{Co}_{1-x}\text{TiO}_3$ precursors suggested that the presence of metallic Pd under the operating conditions favored the electrophilic aromatic substitution of the C–Cl bond of the CAN product to generate AN and HCl as reaction by-products.

However, the catalytic activity mainly depended on the amount of metallic Co. The reduced $(\gamma)\text{Pd-Co/CTO}$ systems with $y = 0.0$ –0.10 showed CAN product selectivities of 100%. Among these, the 0.10Pd-Co/CTO system showed the highest activity. Thus, the 0.10Pd-Co/CTO

system was found to be most favorable for the production of CAN under these conditions.

3.2.2. Hydrogenation of halonitroarenes of pharmaceutical interest

The 0.10Pd-Co/CTO catalyst was tested in the hydrogenation of several halonitroarenes of interest for the production of commercial drugs. Table 4 shows the activity and selectivity of the catalyst. All the substrates showed reaction conversions and chemoselectivities of > 95% for the corresponding haloarene-amines. In the case of 1-(4-chlorophenoxy)-2-nitrobenzene (entry 2) substrate, only a low concentration of the intermediate N-(2-(4-chlorophenoxy)phenyl) hydroxylamine intermediate was detected, ruling out the lateral hydrodechlorination reaction of the C–Cl bond and/or hydrogenolysis of the C–O bond. Only in the case of 2-chloro-1-((3-fluorobenzyl)oxy)-4-nitrobenzene (entry 3) was breakage of the C–O bond to produce the side products 4-amino-2-chlorophenol and 1-fluoro-3-methylbenzene detected. This was attributed to the high activity of Pd in the benzyl-ether hydrogenolysis reaction, which has been reported by Llàcer et al. [61].

3.2.3. Evaluation of the operational stability

The operational stability of the 0.10Pd-Co/CTO system was

evaluated through leachate and recycling tests. All cycles were measured until the maximum conversion time of the fresh catalyst, and the reaction time for the leachate tests was 30 min for each cycle. In the leachate tests, the catalyst was magnetically separated from the reaction medium (at 80 °C) after 30 min of reaction, and the catalytic activity of the supernatant was then determined. In addition, the post-cycle filtrates were analyzed using AAS to quantify the loss of the Pd and/or Co active phases. A summary of the data is shown in Fig. 9A. A continuous decrease in the activity and selectivity of the catalyst was observed, dropping to 75% conversion and 92% selectivity in the third cycle of operation. However, no significant metal activity was detected in the supernatant in the leachate tests (Co and Pd < 10 ppm).

To explain this behavior, XRD characterization of the catalyst recovered after the third cycle of operation was performed, as shown in Fig. 9B. The used catalyst shows diffraction lines for species of the CoOOH-type (ICDD 07-0169), which are associated with the oxidation/hydration of the cobalt metal catalyst during the operation cycles. Although, with the reaction using ethanol as a solvent, one of the hydrogenation products of the -NO₂ group is H₂O, which is generated in situ in the reaction medium and could be responsible for the oxidation of the active phase during operation cycles. Similar results have been reported by Lin et al., who show that the formation of Ni(OH)_x species deactivates the catalyst for hydrogenation in the aqueous phase of nitrobenzene [62].

A catalyst regeneration study was carried out by magnetically separating the catalyst after every two operation cycles and subjecting it to reduction treatment at 500 °C for 3 h. The catalytic activity results of regenerated catalyst are shown in Fig. 10. During the six operation cycles evaluated, continuous selectivity toward CAN was observed (*S* > 98%), but the catalytic activity decreased to 80% conversion in cycle 6 (Fig. 10A). In all the cycles evaluated, there was no significant decrease in the amount of Co and/or Pd in the recovered catalyst. This information suggested that the decreased activity was not due to the leaching of the active phase.

Characterization of the regenerated catalyst (Fig. 10B) revealed a continuous increase in the intensity of the metallic Co diffraction peak in the XRD and the destruction of the micro-rod architecture in the TEM micrographs. The degradation of the catalyst via the formation of CoOOH species and regeneration via thermal reduction could promote sintering of the catalyst, which would be responsible for the loss of catalyst activity.

4. Conclusions

We synthesized supported bimetallic catalysts based on Pd-Co from palladium-substituted cobalt titanates. The catalysts were found to be active and selective in the hydrogenation of halonitroarenes. Compared to the mono-metallic Co catalyst, all the catalysts showed increased hydrogenation activity with the incorporation of palladium. Additionally, we determined that there is an optimal Pd content at which the accumulation of hydrogenation intermediates of the -NO₂ group is inhibited and hydrodehalogenation by-products are not formed. The optimal catalyst also showed high activity and selectivity in the liquid-phase hydrogenation of halonitroarene derivatives of pharmaceutical interest. Finally, operational stability tests showed that the catalyst was deactivated during continuous operation cycles, but could be regenerated for 6 cycles with high selectivity and moderate catalytic activity.

Declaration of Competing Interest

None.

Acknowledgements

The authors thank CONICYT FONDECYT11170095,

FONDECYT1170083, FONDECYT 1191465, Unidad de Equipamiento Científico - MAINI, Universidad Católica del Norte, for the XPS analysis (Conicyt-Programa FONDEQUIP XPS EQM 140044 2014-2016), and Universidad Andres Bello Conicyt-Fondequip/PPMS/EQM130086 for VSM analysis. T. Bustamante thanks to CONICYT Grant 21190739 and R. Dinamarca thanks to CONICYT Grant 21150092 for their PhD fellowship. C.C. Torres thanks to CONICYT, PAI/Concurso Nacional inserción de Capital Humano Avanzado en la Academia Convocatoria año 2017 PAI79170027.

References

- [1] C.H. Bartholomew, R.J. Farrauto, *Fundamentals of Industrial Catalytic Processes*, John Wiley & Sons, Inc., 2005 p. 337.
- [2] N. Pal, A. Bhaumik, M. Fan, J. Wang (Eds.), *Sustainable Catalytic Processes*, Elsevier, Amsterdam, 2015p. 23.
- [3] P. Unnikrishnan, D. Srinivas, V.V. Ranade (Ed.), *Industrial Catalytic Processes for Fine and Specialty Chemicals*, Elsevier, Amsterdam, 2016p. 41.
- [4] J. Song, Z.-F. Huang, L. Pan, K. Li, X. Zhang, L. Wang, J.-J. Zou, *Appl. Catal. B* 227 (2018) 386.
- [5] S.V. Ley, I.R. Baxendale, *Nat. Rev. Drug Discov.* 1 (2002) 573.
- [6] J.L. Vennerstrom, *J. Med. Chem.* 51 (2008) 1502.
- [7] G. Romanazzi, A.M. Fiore, M. Mali, A. Rizzuti, C. Leonelli, A. Nacci, P. Mastrolilli, M.M. Dell'Anna, *Mol. Catal.* 446 (2018) 31.
- [8] W. Shi, B. Zhang, Y. Lin, Q. Wang, Q. Zhang, D.S. Su, *ACS Catal.* 6 (2016) 7844.
- [9] S.S. Kotha, N. Sharma, G. Sekar, *Tetrahedron Lett.* 57 (2016) 1410.
- [10] W. Yu, L.-L. Lou, S. Li, T. Ma, L. Ouyang, L. Feng, S. Liu, *RSC Adv.* 7 (2017) 751.
- [11] M. Lan, B. Zhang, H. Cheng, X. Li, Q. Wu, Z. Ying, Y. Zhu, Y. Li, X. Meng, F. Zhao, *Mol. Catal.* 432 (2017) 23.
- [12] P.A. Bolla, A. Sanz, S. Huggias, J.F. Ruggera, M.A. Serradell, M.L. Casella, *Mol. Catal.* (2018) 110262.
- [13] Y. Guo, J. Li, F. Zhao, G. Lan, L. Li, Y. Liu, Y. Si, Y. Jiang, B. Yang, R. Yang, *RSC Adv.* 6 (2016) 7950.
- [14] M. Tian, X. Cui, C. Dong, Z. Dong, *Appl. Surf. Sci.* 390 (2016) 100.
- [15] L. Jiang, Z. Zhang, *Int. J. Hydrogen Energy* 41 (2016) 22983.
- [16] Y. Duan, M. Zheng, D. Li, D. Deng, C. Wu, Y. Yang, *RSC Adv.* 7 (2017) 3443.
- [17] C.S. Couto, L.M. Madeira, C.P. Nunes, P. Araújo, *Appl. Catal. A Gen.* 522 (2016) 152.
- [18] C.H. Campos, E. Rosenberg, J.L.G. Fierro, B.F. Urbano, B.L. Rivas, C.C. Torres, P. Reyes, *Appl. Catal. A Gen.* 489 (2015) 280.
- [19] C.-H. Péllisson, A. Denicourt-Nowicki, A. Roucoux, *ACS Sustain. Chem. Eng.* 4 (2016) 1834.
- [20] J.J. Martínez, E.X. Aguilera, J. Cubillos, H. Rojas, A. Gómez-Cortés, G. Díaz, *Mol. Catal.* 465 (2019) 54.
- [21] C. Campos, C. Torres, M. Oportus, M.A. Peña, J.L.G. Fierro, P. Reyes, *Catal. Today* 213 (2013) 93.
- [22] T. Higaki, H. Kitazawa, S. Yamazoe, T. Tsukuda, *Nanoscale* 8 (2016) 11371.
- [23] T. Fukutake, K. Wada, H. Yu, S. Hosokawa, Q. Feng, *Mol. Catal.* 477 (2019) 110550.
- [24] C.H. Campos, M. Jofré, C.C. Torres, B. Pawelec, J.L.G. Fierro, P. Reyes, *Appl. Catal. A Gen.* 482 (2014) 127.
- [25] C.C. Torres, J.B. Alderete, G. Pecchi, C.H. Campos, P. Reyes, B. Pawelec, E.G. Vaschetto, G.A. Eimer, *Appl. Catal. A Gen.* 517 (2016) 110.
- [26] P. Serna, A. Corma, *ACS Catal.* 5 (2015) 7114.
- [27] C.C. Torres, V.A. Jiménez, C.H. Campos, J.B. Alderete, R. Dinamarca, T.M. Bustamante, B. Pawelec, *Mol. Catal.* 447 (2018) 21.
- [28] T. Schwob, R. Kempe, *Angew. Chem. Int. Ed.* 55 (2016) 15175.
- [29] L. Xing, J. Qiu, C. Liang, C. Wang, L. Mao, *J. Catal.* 250 (2007) 369.
- [30] L. Liu, P. Concepción, A. Corma, *J. Catal.* 340 (2016) 1.
- [31] J. Xiong, J. Chen, J. Zhang, *Catal. Commun.* 8 (2007) 345.
- [32] J. Chen, N. Yao, R. Wang, J. Zhang, *Chem. Eng. J.* 148 (2009).
- [33] G. Hahn, J.-K. Ewert, C. Denner, D. Tilgner, R. Kempe, *ChemCatChem* 8 (2016) 2461.
- [34] Y. Ren, H. Wei, G. Yin, L. Zhang, A. Wang, T. Zhang, *Chem. Commun.* 53 (2017) 1969.
- [35] A. Hu, X. Lu, D. Cai, H. Pan, R. Jing, Q. Xia, D. Zhou, Y. Xia, *Mol. Catal.* 472 (2019) 27.
- [36] K. Wang, W. Gao, P. Jiang, K. Lan, M. Yang, X. Huang, L. Ma, F. Niu, R. Li, *Mol. Catal.* 465 (2019) 43.
- [37] S. Jian, Y. Li, *Chin. J. Catal.* 37 (2016) 91.
- [38] H. Yang, X. Cui, Y. Deng, F. Shi, *ChemCatChem* 5 (2013) 1739.
- [39] H. Bao, D. Wang, X. Wang, C. Cheng, Y. Li, Y. Hu, *RSC Adv.* 5 (2015) 47125.
- [40] L. Chang, Y. Li, *Mol. Catal.* 433 (2017) 77.
- [41] Y. Bharath, G.R. Alugubelli, R. Sreenivasulu, M.V.B. Rao, *Chem Papers* 72 (2018) 457.
- [42] B.S. Wagh, B.P. Patil, M.S. Jain, S.S. Harak, S.B. Wagh, *Synthesis and evaluation of antipsychotic activity of 11-(4-aryl-1-piperazinyl)-dibenz [b,f][1,4] oxazepines and their 8-chloro analogues*, *Heterocyclic Communications*, (2007) p. 165.
- [43] M. Hossam, D.S. Lasheen, N.S.M. Ismail, A. Esmat, A.M. Mansour, A.N.B. Singab, K.A.M. Abouzid, *Eur. J. Med. Chem.* 144 (2018) 330.
- [44] K.G. Rosauer, A.K. Ogawa, C.A. Willoughby, K.P. Ellsworth, W.M. Geissler, R.W. Myers, Q. Deng, K.T. Chapman, G. Harris, D.E. Moller, *Bioorg. Med. Chem. Lett.* 13 (2003) 4385.

- [45] J. Yao, Z. He, J. Chen, W. Sun, H. Fang, W. Xu, *Bioorg. Med. Chem. Lett.* 22 (2012) 6549.
- [46] Y. Qu, W. Zhou, H. Fu, *ChemCatChem* 6 (2014) 265.
- [47] R. Morales, C.H. Campos, J.L.G. Fierro, M.A. Fraga, G. Pecchi, *Catal. Today* 310 (2018) 59.
- [48] J.H. Hwang, E.N. Son, R. Lee, S.H. Kim, J.I. Baek, H.J. Ryu, K.T. Lee, J.M. Sohn, *Catal. Today* 303 (2018) 13.
- [49] M. Vafaei, M. Rezaei, S.H. Tabaian, F. Mahboubi, D.F. Haghshenas, *J. Solid State Electrochem.* 19 (2015) 289.
- [50] R. Dinamarca, R. Espinoza-González, H.C. Campos, G. Pecchi, *Materials* 12 (2019).
- [51] V.A. de la Peña O'Shea, M. Consuelo Álvarez Galván, A.E. Platero Prats, J.M. Campos-Martin, J.L.G. Fierro, *Chem. Commun.* 47 (2011) 7131.
- [52] G. Yang, W. Yan, J. Wang, H. Yang, *Mater. Lett.* 122 (2014) 117.
- [53] Y. Bi, G. Lu, *Appl. Catal. B* 41 (2003) 279.
- [54] P. Fu, P. Zhang, J. Li, *Appl. Catal. B* 105 (2011) 220.
- [55] J.-N. Zheng, L.-L. He, F.-Y. Chen, A.-J. Wang, M.-W. Xue, J.-J. Feng, *J. Mater. Chem. A* 2 (2014) 12899.
- [56] Y. Ma, R. Wang, H. Wang, J. Key, S. Ji, *RSC Adv.* 5 (2015) 9837.
- [57] H. Wu, Y. Yang, H. Suo, M. Qing, L. Yan, B. Wu, J. Xu, H. Xiang, Y. Li, *J. Mol. Catal. A Chem.* 390 (2014) 52.
- [58] A. Henglein, *J. Phys. Chem. B* 104 (2000) 6683.
- [59] S. Özkar, R.G. Finke, *Langmuir* 32 (2016) 3699.
- [60] D.P. Dissanayake, J.H. Lunsford, *J. Catal.* 214 (2003) 113.
- [61] E. Llàcer, P. Romea, F. Urpí, *Tetrahedron Lett.* 47 (2006) 5815.
- [62] W. Lin, H. Cheng, J. Ming, Y. Yu, F. Zhao, *J. Catal.* 291 (2012) 149.